Published in final edited form as:
J Cell Physiol. 2012 June ; 227(6): 2542–2555. doi:10.1002/jcp.22992.

NIFLUMIC ACID BLOCKS NATIVE AND RECOMBINANT T-TYPE CHANNELS

E Balderas[1], **R Arteaga-Tlecuitl**[2], **M Rivera**[2], **JC Gomora**[2], and **A Darszon**[1,*]

[1]Departamento de Genética del Desarrollo y Fisiología Molecular, Instituto de Biotecnología, Universidad Nacional Autónoma de México (UNAM). Avenida Universidad 2001, Col. Chamilpa, C.P. 62210, Cuernavaca Mor., México

[2]División de Neurociencias, Instituto de Fisiología Celular, UNAM, México DF, México

Abstract

Voltage-dependent calcium channels are widely distributed in animal cells, including spermatozoa. Calcium is fundamental in many sperm functions such as: motility, capacitation and the acrosome reaction, all essential for fertilization. Pharmacological evidence has suggested T-type calcium channels participate in the acrosome reaction. Niflumic acid (NA), a non-steroidal anti-inflammatory drug commonly used as chloride channel blocker, blocks T-currents in mouse spermatogenic cells and Cl^- channels in testicular sperm. Here we examine the mechanism of NA blockade and explore if it can be used to separate the contribution of different Ca_V3 members previously detected in these cells. Electrophysiological patch-clamp recordings were performed in isolated mouse spermatogenic cells and in HEK cells heterologously expressing Ca_V3 channels. NA blocks mouse spermatogenic cell T-type currents with an IC_{50} of 73.5 μM, without major voltage-dependent effects. The NA blockade is more potent in the open and in the inactivated state than in the closed state of the T-type channels. Interestingly, we found that heterologously expressed $Ca_V3.1$ and $Ca_V3.3$ channels were more sensitive to NA than $Ca_V3.2$ channels, and this drug substantially slowed the recovery from inactivation of the three isoforms. Molecular docking modeling of drug-channel binding predicts that NA binds preferentially to the extracellular face of $Ca_V3.1$ channels. The biophysical characteristics of mouse spermatogenic cell T-type currents more closely resemble those from heterologously expressed $Ca_V3.1$ channels, including their sensitivity to NA. As $Ca_V3.1$ null mice maintain their spermatogenic cell T-currents, it is likely that a novel $Ca_V3.2$ isoform is responsible for them.

Keywords

Niflumic acid; T-type channels; Blockade Mechanism

INTRODUCTION

Alterations in intracellular Ca^{2+} concentration ($[Ca^{2+}]_i$) are fundamental transduction elements in cell signalling. Voltage-dependent Ca^{2+} channels (Ca_V) translate membrane

*Corresponding author: Alberto Darszon. darszon@ibt.unam.mx, Phone: +52 777 3291650, Fax: +52 777 3172388.

potential (V_m) changes into intracellular Ca^{2+} signals. There are two major classes of Ca_V channels; the Low (LVA) and the High Voltage-Activated (HVA) channels. Strong depolarizations in V_m are needed to open HVA channels, which inactivate slowly and are classified into L-, N-, P/Q- and R- types depending on their biophysical properties (Perez-Reyes 2003). In contrast, LVA channels open transiently in response to weak depolarizations and inactivate faster than HVA channels, therefore they were named T-type channels (for **T**ransient). LVA channels have been identified in several tissues, including neural tissue, heart, kidney, smooth muscle, skeletal muscle and sperm (for review see Perez-Reyes 2003; Darszon et al., 2006). In neurons for instance, they play a role as a pacemaker, inducing low-threshold spikes which in turn may trigger a burst of action potentials mediated by Na^+ channels (Sherman, 2005; Steriade, 2005; Perez-Reyes 2003).

Direct Ca^{+2} entry through T-type channels modulates $[Ca^{2+}]_i$, which plays a key role in the regulation of fundamental processes in many cells, including sperm (Darszon et al., 2011). The mRNAs and the proteins of the complete family of T-type channels (α1G or Ca_V3.1, α1H or Ca_V3.2 and α1I or Ca_V3.3), have been found in both mammalian spermatogenic as well as mature sperm cells (Espinosa et al., 1999; Son et al., 2000 and 2002; Jagannathan et al., 2002; Park et al., 2003; Trevino et al., 2004; Darszon et al., 2006; Escoffier et al., 2007), although electrophysiological and pharmacological evidences suggest that Ca_V3.2 might be the main subunit carrying the T- type current in spermatogenic cells (Lievano et al., 1996; Arnoult et al., 1996; Santi et al., 1996; Espinosa et al., 1999; Stamboulian et al., 2004; Escoffier et al., 2007). However, distinguishing macroscopic currents among Ca_V3.2 and the other two Ca_V3 members (Ca_V3.1 and Ca_V3.3), requires a detailed analysis of specific parameters already described for recombinant channels such as recovery from inactivation (Perez-Reyes 2003), and/or their sensitivity to chemical compounds. For instance, Ni^{2+} blockade of the spermatogenic cell T-type current showed two components, one clearly attributed to Ca_V3.2, and a second due to Ca_V3.1 or Ca_V3.3 or both channels (Trevino et al., 2004).

In genetic studies, Ca_V3.1 knockout mice did not show any alteration to their T-type currents in spermatogenetic cells; in contrast, these same cells in Ca_V3.2 null mice lack T-type currents, supporting the idea that Ca_V3.2 is the main active Ca_V3 isoform in spermatogenic cells (Stamboulian et al., 2004). As Ca_V3.2 null mice are fertile, compensation for the missing subunit in male gametes of knockout mice should be considered likely. Under this perspective, finding compounds which selectively block the specific T-type channel isoforms would be very useful, in general, to discriminate their participation in physiological processes.

The acrosome reaction (AR) is obligatory prior to fertilization and is highly dependent on extracellular Ca^{2+}. There is evidence both supporting and against the participation of T-type channels in this reaction (Darszon et al., 2006; Escoffier et al., 2007; Ren and Xia, 2010). Although macroscopic T-type currents are present in testicular sperm (Martínez-Lopez et al., 2008), they disappear in more mature non-capacitated epididymal sperm (Ren and Xia, 2010) for unknown reasons. In spite of this, the mouse AR closely follows the pharmacology of spermatogenic cell and testicular sperm Ca_V3 channels, suggesting they have a pivotal role in the $[Ca^{2+}]_i$ increments required for this reaction.

Niflumic acid (NA) is a non-steroidal anti-inflammatory drug that effectively blocks T-type currents in spermatogenic cells from mice (Espinosa et al., 1999). Interestingly, NA was found to prevent AR triggered by GABA, ZP, and progesterone (Espinosa et al., 1998). NA displays a similar IC_{50} (~85 μM) in inhibiting both the AR triggered by progesterone and the T-type currents in spermatogenic cells (IC_{50}~45 μM) as previously described (Espinosa et al., 1999). Mouse spermatogenic cells mainly display Ca_V3 currents with pharmacological characteristics resembling those of the transient Ca^{2+} uptake that occurs during the ZP-induced AR (Arnoult et al., 1996). This evidence suggests that T-type channels may participate in the AR in mice; therefore elucidating the mechanism of NA blockade could be useful to understand their participation in fertilization. In addition, as we mentioned above, determining the sensitivity of each of the three T-type recombinant isoforms to NA could uncover the potential of this compound to dissect their individual contribution in native systems such as spermatogenic cells.

Furthermore, the blocking mechanism of T-type channels by NA has not been studied extensively. In this work we characterize the blocking of T-type currents by this inhibitor in spermatogenic cells, and extend the study to the three recombinant T-type channels stably expressed in HEK-293 cells, and examine the blocking and molecular docking properties of the drug. Macroscopic T-type currents in spermatogenic cells could be the result of the mixed activity of the three T-type channels: $Ca_V3.1$, $Ca_V3.2$ and $Ca_V3.3$, already identified in these cells (Trevino et al., 2004; Darszon et al., 2006). Our results show that blockade by NA is not voltage-dependent and is partially reversible, which suggest a weak interaction with its binding site. We observed that this effect is not use dependent, but depends on the state of the channel. Our findings also indicate that NA strongly delays recovery from inactivation of Ca_V3 channels when studied in both spermatogenic and HEK-293 stably transfected cells. The time course of recovery from inactivation and the sensitivity to NA of the T-type currents of spermatogenic cells suggest that $Ca_V3.1$ channels may significantly contribute to the current. Alternatively, as ~15% of the T-type current remained insensitive to 1 mM of NA in spermatogenic cells, either another Ca_V isoform displaying unknown regulatory mechanisms could exist in this native environment.

METHODS

Dissociation procedure

Spermatogenic cells were obtained as described (Santi et al., 1996). Briefly, seminiferous tubules were isolated from adult male mice testes (three months old) and washed out several times in Ca^{2+}-free saline solution. To isolate the spermatogenic cells, tubules were compressed with a 3 ml transfer pipette. Isolated cells were placed in a Plexiglas recording chamber on the stage of an inverted microscope (Eclipse 2000, Nikon, Japan). Once the cells were attached to the bottom of the chamber, external solution was continuously superfused at a rate of 2ml/min.

Electrophysiology of spermatogenic cells

Ca^{2+} currents were recorded in mouse spermatogenic cells using the whole cell configuration of the patch-clamp technique as described previously (Santi et al., 1996;

Espinosa et al., 1999, Trevino et al., 2004). Briefly, currents were recorded with an Axopatch 200A amplifier (Molecular Devices, Sunnyvale, CA), filtered with a corner frequency of 2 kHz (four-pole Bessel filter), digitized at 10 kHz using a Digidata 1200A (Molecular Devices), and stored on a personal computer. Cells were bathed in a solution containing (in mM): 2 $CaCl_2$; 130 NaCl; 3 KCl; 2 $MgCl_2$; 1 $NaHCO_3$; 0.5 NaH_2PO_4; 5 HEPES; 10 glucose, pH 7.3. The bath was grounded with an Ag-AgCl pellet. The internal solution consisted of (in mM): 120 $CsMeSO_3$; 10 CsF; 15 CsCl; 5 EGTA; 5 HEPES; 4 Mg-ATP; 10 phosphocreatine, pH 7.3. Internal Cs^+ by itself effectively blocked the majority of outward K^+ currents. Open-tip pipettes had resistances ranging between 8 and 10 MΩ when filled with pipette solution. Data were obtained from cells where the product of uncompensated series resistance and peak current was less than 5 mV, which was not corrected. Pulse generation, data acquisition and analysis were done using computer-driven software (pCLAMP 9.0; Molecular Devices). Capacitive transients were electronically compensated, and leak currents were subtracted on-line using a P/4 protocol. Experiments were conducted at room temperature (22–25°C).

Niflumic acid (2-{[3-(trifluoromethyl) phenyl] amino}- pyridine-3-carboxylic acid) (NA) was purchased from Sigma-Aldrich (St. Louis, MO) and was prepared as a 50 mM stock solution in DMSO. An aliquot of this stock was dissolved in the bath solution immediately before use to obtain the final desired drug concentrations. The control solution always contained the same quantity of DMSO as the bath with NA solution (e.g., 0.1% DMSO for 500 μM NA).

Current-voltage (*I–V*) relationships for T-type channels were determined by applying 350 ms depolarizing pulses from −80 to +70 mV, in 10 mV increments, from a holding potential (HP) of −90 mV, every 5 s. Recording protocols were applied before (control) and after the superfusion of the drug at a rate of 2 ml/min. Activation and inactivation current kinetics were fitted by standard exponential functions. Drug-induced current reduction was assessed by measuring maximum inward current (peak current) of the 350 ms depolarizing pulse to −20 mV, and calculating the percentage reduction relative to the control current at each NAconcentration tested (0.5 to 1000 μM). Dose-response curves were fitted with a Hill equation:

$$y=a/[1+(X/X_0)^b]$$

Where *a*, *b* and X_0 represent the *y*-intercept, the slope, and the IC_{50} value, respectively. The voltage dependence of T-type current activation was estimated using a modified Boltzmann function to fit *I–V* data:

$$I_{\mathrm{Ca}}=I_{\max}(V_{\mathrm{m}}-V_{\mathrm{rev}})/(1+\exp\,((V_{50}-V_{\mathrm{m}})/k)$$

Where I_{Ca} is the peak current, V_m is the test potential, V_{rev} is the apparent reversal potential, V_{50} is the mid-point of activation, and *k* is the slope factor. To determine whether NA preferentially blocks any specific state of the T-type channels, we applied a test pulse to −20 mV from a HP of −90 mV, taking the record without drug as a control. Then we

hyperpolarized the cells to −90 mV, added 100 μM of NA and waited for 120 s to remove inactivation and have the majority of the channels in the closed state. Then we re-opened the channels with another pulse of −20 mV to evaluate the percent of blockade by NA. For the inactivated state cells were maintained to a HP= −20 mV after a first round of opening without drug (control) and we added NA at this stage, after this a 400 ms hyperpolarized pulse of −90 mV was applied every 120 s to remove inactivation of the channels followed by a depolarized pulse of −20 mV to opened the channels again and evaluated the percent of blockade current. To record the effect of NA on the open state of the channels we applied depolarized pulses of −20 mV every 5 s from a HP= −90 mV in the absence (control) and in the presence of NA. Steady-state inactivation curves were obtained by normalizing the current values acquired from a typical two-pulse protocol, and fitting the data with a Boltzmann equation:

$$I_{\mathrm{ca}}=I_{\max}/(1+\exp\,((V-V_{50})/k)),$$

where I_{Ca} is the peak current at the test potential (−20 mV), I_{max} is the peak current at −20 mV when the pre-pulse was at −110 mV, V is the inactivating pre-pulse potential, V_{50} is the half-inactivation value and k is the inactivation steepness parameter.

Expression of recombinant Ca_V3 channels and electrophysiology

Human embryonic kidney (HEK-293) cells stably transfected with human α1G channel or $Ca_V3.1$ (Gen Bank Accession No. AF190860), human α1H channel or $Ca_V3.2$ (AF051946) and human α1I channel or $Ca_V3.3$ (AF393329), were grown in Dulbecco's modified Eagle's medium (DMEM) supplemented with 10% fetal bovine serum, 100U/ml penicillin, and 100 μg/ml streptomycin at 37 °C in a CO_2 incubator. Selection of cells expressing the channels was maintained by adding 1 mg ml^{-1} of G-418 to the culture medium. All cell culture reagents were purchased from Gibco-Life Technologies (Grand Island, NY). Whole-cell Ca^{2+} currents were recorded at room temperature (21–23°C), according to the patch-clamp technique (Hamill *et al.*, 1981) by using an Axopatch 200B amplifier, a Digidata 1320 A/D converter, and the pCLAMP 9.0 software (Molecular Devices). Currents were usually digitized at 10–kHz, following 2–kHz analog filtering, except for tail currents which were sampled at 100 kHz and filtered at 10 kHz. Whole-cell series resistance (initially 3.5 ± 0.2 MΩ, n = 33), and cell capacitance (19.6 ± 1.3 pF, n = 33) was estimated from optimal cancellation of the capacitive transients with the built-in circuitry of the amplifier, and was compensated electrically by 60–70%. The HP was −100 mV. In most cases, currents were recorded on two channels, one with on-line leak subtraction using the P/-5 method, and the other to evaluate cell stability and holding current. Only leak subtracted data are shown. Cells were bathed in a solution containing (in mM): 2 $CaCl_2$; 160 tetraethyl ammonium (TEA) chloride; and 10 HEPES (pH 7.4). The internal (pipette) solution contained (in mM): 135 CsCl; 10 EGTA; 4 Mg-ATP; 0.3 Tris-GTP; and 10 HEPES (pH 7.3). NA was prepared as mentioned for spermatogenic cells. However, in this case the effect of DMSO (0.2%) on Ca_V3 channels was assessed before exposing the channels to NA. DMSO by itself reduced the calcium current amplitude by 10 ± 3, 13 ± 2 y 8 ± 3% of $Ca_V3.1$, $Ca_V3.2$ and $Ca_V3.3$ channels. The NA blocking data shown in the results section is additional to this effect.

Calculation of K_d values from the fractional blocking of Ca_V3 channels by 100 μM NA was performed with the following function:

$$Y=T/T+K_d$$

Where, Y is the fraction of blocked current by NA, T is the NA concentration and K_d is the dissociation constant of the NA-channel complex.

Current recordings were analyzed with Clampfit 9.0, and averaged data (mean ± standard error; SEM) was obtained with Lotus 123 and Excel. Differences in means were tested with unpaired two-tailed Student´s *t*-test and were accepted as significant if $P < 0.05$. Final graphs were plotted with Prism 5.0 software.

Molecular Docking

The three-dimensional structure of Ca_V3 channels was obtained from homology modeling by MODELLER (Fiser and Sali, 2003) using the PDB structures 1K4C (Zhou *et al.*, 2001), 3NLM (Ji *et al.*, 2010) and 1BL8 (Doyle *et al.*, 1998) as templates. Also, the automated I-TASSER server was used to obtain *ab initio* models (Roy *et al.*, 2010). Channel models were generated only for the pore domain (S5, S6 and pore linker from the four repeats). The PDBePISA program (Krissinel, 2010) was used to extract a monomer from the tetramer structure of 1K4C, and to perform the structural search of a similar interface of the likely assembly. Then MGLTools v1.5.2 (Sanner, 1999) was used to assign Gasteiger charges to the protein and to generate the structural file for docking. The chemical structure of NA (CID: 4488) was obtained from the NCBI PubChem Compounds Database (http://www.ncbi.nlm.nih.gov/pccompound). The structure of the ligand was constructed and prepared for docking with the program Open Babel 2.3.0 (Guha *et al.*, 2006). A combination of rigid receptor and flexible ligand protocols were used in the docking process using Auto Dock/Vina 1.1.1 (Trott and Olson, 2010) in the exhaustiveness mode 9, using two Dual-core processors. Affinity grids on the binding pocket were constructed using AutoGrid4 (Morris et al., 1998), with grid spacing to $Ca_V3.3$: center_x=35.202; center_y=35.361; center_z=20.036; size_x=126; size_y=104; size_z=114; to $Ca_V3.2$: center_x=155.56; center_y=139.44; center_z=−16.62; size_x=102; size_y=126; size_z=104; to $Ca_V3.1$: center_x=155.46; center_y=139.44; center_z=−16.62; size_x=102; size_y=126; size_z=104;and to 1K4C; center_x=156.817; center_y=150.483; center_z=−25.374; size_x=126; size_y=34; size_z=126. Final docked structures were visualized, analyzed and rendered using PyMOL (DeLano, 2002).

RESULTS

NA blocks T-type calcium currents in spermatogenic cells

We have shown previously that under the experimental conditions employed in this work, the calcium currents in spermatogenic cells are carried exclusively through T-type calcium channels (Liévano et al., 1996; Santi et al., 1996; Arnoult et al. 1996). Considering that NA is able to block acrosomal reaction, and effectively blocks T-type channels in spermatogenic

cells, determination of the mechanism of blockade by this drug would clarify the participation of Ca_V3 channels under physiological conditions.

To confirm the presence of T-type currents we stimulated spermatogenic cells with test pulses from −80 to +30 mV from a HP of −90 mV (Fig. 1*A*). Under control conditions, activation of inward current was observed at potentials more positive than −60 mV, with a maximum peak current between −30 and at −20 mV. These currents activated and inactivated within a few milliseconds (~ 50 ms), showing the typical criss-crossed pattern of T-type currents (Fig. 1*A*). We then determined the dose-response curve for NA in spermatogenic cells. It is important to mention that around 15% of the T-type current remained insensitive to 1 mM of NA, and thus we normalized its inhibition to the maximum block observed at this NA concentration. Averaged fractional blockade values at different NA concentrations were fitted with a Hill equation, obtaining an IC_{50} of 73.5 μM (Fig. 1*B*). Then, we explored the effect of 100 μM NA on T-type currents within a range of voltages from −80 to +30 mV in 10 mV steps, observing a reduction of the inward current at all the voltages tested (Fig. 1*C*). Analysis of *I–V* curves revealed a ~ 50% reduction in the normalized T-type current amplitude by NA in most of the explored potentials (Fig. 1*D*), without significant changes in the voltage dependence of current activation; although there was a small change (4 mV) in V_{rev} toward negative potentials.

NA did not affect steady-state inactivation of T-type calcium channels

To investigate if NA changes the steady-state of inactivation we applied inactivating pulses from −110 to −40 mV in 5 mV steps before a test pulse to −20 mV (Fig. 2*A* top). Again, when compared with Control currents (Fig. 2*A*), there was a clear reduction in the current amplitude in the presence of 100 μM NA (Fig. 2*B*). Steady-state inactivation curves were constructed for the Control and NA conditions (Fig. 2*C*) by normalizing current amplitudes to the maximum current recorded at −20 mV under the corresponding condition. Data points were fitted with a Boltzmann relationship (Fig. 2*C*). Control current inactivation occurs between −80 and −50 mV, with a half-inactivation potential (V_{50}) of −63.9 ± 0.3 mV and a steepness parameter (k) of 2.8 ± 0.27 mV (n = 9); while in the presence of 100 μM NA the values were: V_{50} = −64.4 ± 0.5 mV and k = 3.7 ± 0.48 mV. The lack of effect of NA on the steady-state inactivation and activation curves (Fig. 1*D*) suggests that the binding site of the drug is not affecting the voltage sensor (S4).

NA slows down T-type current activation and inactivation kinetics

T-type Ca^{2+} currents activate within a few ms (>15 ms) in response to depolarizing potentials more positive than −60 mV from a HP= −90 mV (Fig. 3*A*). However, in the presence of 100 μM NA, T-type current activation and inactivation showed slightly slower kinetics (Fig. 3*B*). T-type currents obtained at different potentials were fitted with two exponentials, one for the activation and another for the inactivation process (Fig. 3*B*, bottom traces). The obtained time constants, τ_{act} and τ_{inact} were plotted against the test potential in Control and NA conditions (Fig. 3*C*, *D* respectively). In both conditions, τ_{act} accelerates monotonically within −50 to +20 mV, and then becomes practically voltage independent between −20 to +20 mV (Fig. 3*C*). Overall, NA slows down activation kinetics of the T-type current, particularly at voltages between −40 and −20 mV (Fig. 3*C*, open symbols). This

result suggests that blockade by NA significantly slows opening of the channels, mainly at potentials where the maximum activity of the channels was recorded (−30, −20 mV). Notably, NA affected τ_{inact} in the same direction, as inactivation became significantly slower at all voltages, except −60 mV (Fig. 3*D*, open symbols). Although τ_{act} is modified by NA, the voltage dependence of activation is not shifted suggesting an interaction of NA with channel gating that slightly slows the opening kinetics but does not interact with the S4 segment. On the other hand, the effects on the inactivation kinetics can be explained by assuming that NA slows down the conformational changes required for the open-to-inactivated transition of the channel. These results clearly suggest a mechanism of blockade that depends on the state of the channel.

NA did not affect deactivation kinetics of T-type calcium current

The effect of NA on T-type channel closing in spermatogenic cells was evaluated by measuring the tail current decay rate at different repolarizing potentials. The time constant of deactivation (τ_{deact}) showed a strong voltage-dependence, with values from 2.4 ± 0.5 ms at −120 to 5.6 ± 1.1 ms at −80 mV, however these values were not significantly different from those obtained after the addition of 100 μM NA (3.3 ± 0.7 ms at −120 and 8.9 ± 2.3 ms at −80 mV; $n = 9$). This result indicates that NA does not interfere with the closing of T-type channels (not shown).

Block of T-type current by NA depends on the state of the channel

To investigate if blockade of T-type channels by NA was preferentially from the open, closed or the inactivated state of the channel, we recorded calcium currents by applying voltage protocols designed specifically for each state of the channel. First, for the closed state, spermatogenic cells were held at −90 mV and depolarized to −20 mV. Control current was recorded without drug (Fig. 4*A* left panel) then cells were perfused with 100 μM NA and maintained at −90 mV during 120 s. After this time channels were re-opened by applying a second pulse to −20 mV, which evocates a current whose amplitude was ~ 25% smaller than the Control recorded (Fig. 4*A*, left panel). This reduction of T-type current by NA in the closed state of the channel remained practically unchanged even after 10 min of exposure to the drug (Fig. 4*A*, right panel). Second, to explore the NA effect on the inactivated state, T-type channels were opened at −20 mV and the potential was held at this level. The current recorded without the drug was taken as Control. Then, with the HP still at −20 mV, NA was added and its effect measured after 2 min by applying a 400 ms prepulse to −90 mV followed by a test pulse to −20 mV (Fig. 4*B*, left panel). The presence of NA induced a ~ 50% reduction in the current amplitude when compared to Control (Fig. 4*B*, right panel). In third place, to explore whether NA blocks T-type channels in the open state, cells were depolarized to −20 mV every 5 s from an HP of −90 mV. This protocol promotes channels to pass frequently through the open state. The first ten pulses recorded without drug were taken as control currents (Fig. 4*C*, black lines left panel). Addition of NA induced a gradual reduction of inward currents reaching a maximum within the first 120 s of exposure (Fig. 4*C*, grey traces and right panel). The ~ 50% reduction of inward current observed was due to the blockade by NA rather than a run-down effect, as revealed by the unchanged currents in the absence of the drug (Fig. 4*C*, inset). In all cases about 85 % of the original current was recovered by wash-out of the drug (Fig. 4*A*, *B* and *C* right panels). All

these results indicate that NA interacts preferentially with the open and/or inactivated state of T-type channels rather than with the closed state, suggesting that NA could also affect recovery from inactivation of T-type channels.

NA delays T-type current recovery from inactivation

To test the possibility whether NA affects the time course of recovery from inactivation we applied a classical two-pulse protocol from a HP of −100 mV. Currents were evoked by depolarizations to −20 mV separated from each other by increasing 10-ms periods of time at −100 mV (Δt = 10 ms) (Fig. 5*A*). Normalized current versus time at −100 mV was plotted and experimental data was fitted with a simple exponential. Under control conditions, the calculated time constant of recovery (τ_h) was 67.7 ± 3ms, n = 9 (Fig. 5*A*; Table 1). In the presence of NA, besides the amplitude reduction in the inward current (Fig. 5*B*), the respective τ_h showed a dramatic four-fold increment (318.0 ± 20 ms, n = 9) (Fig. 5*B*; Table 1). In this case, NA blockade of T-type currents was irreversible in most of the cells. Our overall findings are consistent with a mechanism of blockade that involves the interaction of the drug with the inactivation process, rather than with voltage-dependence of channel opening.

Blockade of T-type current by NA is not use dependent

After observing a maximum blockade by NA when T-type channels were stimulated constantly (Fig. 4*C*), we examined if this drug's effect was use dependent by depolarizing the membrane to −20 mV with frequencies ranging from 1 to 3 Hz. After 30 pulses, inward current amplitude was not affected when applying one depolarization per second (1Hz) in the absence or the presence of NA (Fig. 6*A*). On the contrary, with stimulation frequencies of 2 Hz (Fig. 6*B*) and 3 Hz (Fig. 6*C*), the T-type current showed a reduction of 15 and 40%, respectively, between the first and the second pulses applied under control conditions. In both cases, current amplitude reached a plateau within 30 pulses due to the accumulation of inactivation. However, no significant differences were observed when NA was perfused through the recording chamber (Fig. 6, right panels). Therefore NA does not induce further block with the constant stimulation of the channels, as expected for a use-dependent mechanism of blockade.

NA blocks T-type channels in a stably-expressing cell line

To investigate whether the effect of NA observed on the T-type current of spermatogenic cells was selective for any of the three recombinant T-type channels described so far, α1G or $Ca_V3.1$, α1H or $Ca_V3.2$, and α1I or $Ca_V3.3$; we performed patch clamp experiments in separate HEK-293 cell lines stably expressing one of these channels. Inward Ca^{2+} currents evoked by step depolarizations from HP= −100 mV to −40 mV were blocked differentially by 100 μM NA depending of the expressed Ca_V3 channel subtype. The most sensitive to NA was $Ca_V3.1$ (56 ± 3%), while $Ca_V3.2$ and $Ca_V3.3$ both displayed a lesser reduction in their currents (34 ± 5 and 42 ± 3%, respectively) (Fig.7*B*). In most of the studied cells, the block by NA was partially reversible (Fig. 7*A*). We next sought to determine whether the current blockade by NA was accompanied by changes in channel gating. Figure 8*A* shows representative traces of evoked currents by depolarizations to test potentials between −80

and +100 mV (10 mV steps), before and during exposure to 100 μM NA in a HEK-293 cell expressing $Ca_V3.2$ channels. Current inhibition by NA was observed clearly for inward currents, although the potential for the maximal inward current (−40, −30 mV for $Ca_V3.3$) was not modified. Noteworthy, the outward current amplitudes were practically the same in both experimental conditions, mainly for $Ca_V3.1$ currents. By applying the same protocol as in Fig. 8*A*, we obtained data from HEK-293 cells expressing $Ca_V3.1$, $Ca_V3.2$, and $Ca_V3.3$ channels. Peak current in each episode was measured, averaged, and then plotted as a function of the test potential to generate the respective *I–V* relationships (Fig. 8*B*, *C* and *D*). Current became detectable at −70 mV, peaked near −40 mV, and reversed at around +25 mV (+10 mV for $Ca_V3.1$ channels). Modified Boltzmann functions (see Methods) fitted to inward current data points revealed that NA did not modify the voltage-dependence of Ca_V3 channel activation (Table 1). In fact, blockade percentage of $Ca_V3.2$ channels by NA was very similar within the range of −60 to 0 mV (25 ± 9 and 33 ± 9%). However $Ca_V3.1$ and $Ca_V3.3$ displayed larger changes in the same interval of potentials, from 48 ± 4 to 74 ± 9% and from 47 ± 5 to 31 ± 4%, respectively (Fig. 8*E*).

As mentioned before, outward currents through Ca_V3 channels were clearly less sensitive to the block by NA, this was independent of the percent block observed for inward currents, and it was detected in the three T-type channels studied (Fig. 8*B*, *C* and *D*). This result suggests that NA might be binding to an external site in the permeation pathway of the Ca_V3 channels, resulting in a reduction of the whole cell current mostly for inward currents, while outward currents were practically unaffected.

To further investigate the observation that activation kinetics seemed to be slowed down in the presence of NA, current recordings as shown in Fig. 7*A* were also fitted with two exponentials as mentioned above for native currents (Fig. 3B), and the results are shown in Fig. 9*A*, *B* and *C*. As previously reported (Perez-Reyes 2003), the activation of the three Ca_V3 channels was strongly voltage-dependent within membrane potentials between −60 and −10 mV. Also, the time constants show the significant kinetic differences between $Ca_V3.3$ and the other two members of the Ca_V3 family (~ 3-fold slower for the $Ca_V3.3$ kinetics). In the presence of 100 μM NA, the activation kinetics of $Ca_V3.1$, $Ca_V3.2$, and $Ca_V3.3$ channels was clearly slowed down, mostly at voltages between −60 and −20 mV, and particularly for $Ca_V3.2$ and $Ca_V3.3$ (Fig. 9*A–C*, Table 1). On the contrary, inactivation time constants were practically the same in the absence or presence of NA (Fig. 9*A*, *B* and *C*, insets). This last result differs from that observed in spermatogenic cells, where inactivation kinetics was clearly slowed down in the presence of NA (Fig. 3). On the other hand, steady-state inactivation and deactivation kinetics of recombinant Ca_V3 channels were not modified by 100 μM NA, which is consistent with our observations in spermatogenic cells.

Finally, the effect of NA on the recovery from inactivation observed in spermatogenic cell T-currents was also found in Ca_V3 channels (Fig. 10). This property was strongly modified in $Ca_V3.2$ channels (Fig. 10*A*, *B*); although $Ca_V3.1$ and $Ca_V3.3$ showed also a delay in the time course of recovery from inactivation at −100 mV (Fig. 10*B*, *D*; Table 1). Interestingly, even the recovery from inactivation observed in both recombinant and native cells is affected to a similar extent by NA the tau of recovery obtained from spermatogenic cells

under control conditions is closer to that recorded for recombinant $Ca_V3.1$ under the same conditions.

In order to investigate the putative binding of NA molecules to Ca_V3 channel proteins, we have built 3-D structures of Ca_V3 channels pore domain by homology modeling (Rivera and Gomora, 2011, data not published) against the template structures of 1K4C, 3NL and 1BL8, and performed molecular docking of NA to them. The NA molecule was blind docked to the protein models of Ca_V3 channels. Thirty-two docked modes were analyzed for each NA/channel combination. For each docking position, the distance (RMSD l.b., in Å) and the average binding energy (kcal/mol) for the interaction NA/models was obtained and computed. Docking of TEA to the KcsA potassium channel (Doyle *et al.*, 1998) was used as positive control (average binding energy of −3.4 kcal/mol, and distance of 2.99 Å), suggesting a very close interaction between TEA and the KcsA protein model; however when NA was docked to the KcsA channel the distance of the molecule to the protein was considerably greater (19.55 Å), and the average binding energy was also appreciable (−4.1 kcal/mol). The combination of both parameters is an example of a low affinity interaction (Fig. 11). The highest average binding energy was observed for $Ca_V3.1$ channels (−9.14 kcal/mol), which also showed the largest blockade by NA; whereas $Ca_V3.2$ presented an energy value closer to $Ca_V3.3$ (−8.5 and −8.16, respectively). In addition, the shortest distance in NA docking was found with $Ca_V3.3$ channels (7.08 Å), compared with the 10.4 and 13.2 Å for $Ca_V3.1$ and $Ca_V3.2$, respectively. Therefore, the smaller distance found for $Ca_V3.3$ could explain its higher sensibility to NA when compared with $Ca_V3.2$, whose combination of docking parameters are related to a modest blockade by NA.

Further analysis of the docking data included the dissection of the pore domain models in four clusters (Fig. 11*B*). The ratio between binding energy and the distance of each docking position was averaged for each cluster and plotted for each channel (Fig. 11*C*). The data showed that NA binds preferentially to the extracellular face of $Ca_V3.1$ channels, and to the pore itself of $Ca_V3.3$. On the contrary, NA did not bind preferentially to any cluster of $Ca_V3.2$ channel protein.

Discussion

T-type Ca^{2+} channels are fundamental signaling elements in many cell types (Perez-Reyes 2003) and they have been detected in mammalian spermatogenic cells and sperm (Darszon et al., 2011). To date, Ca_V3 channel participation in sperm physiology is a continuing source of debate. In this regard, a drug that can distinguish between Ca_V3 channel isoforms is useful to determine those potentially involved in sperm physiology. Several groups including ourselves have contributed to the idea that $Ca_V3.2$ is the main active Ca_V channel in mouse and human spermatogenic cells and in mouse testicular sperm, and that these channels participate in the AR (Arnoult et al., 1998; Benoff et al., 2007; Darszon et al., 2006; 2011; Jagannathan et al., 2002; Escoffier et al., 2007). In spite of this, $Ca_V3.2^{-/-}$ mice are fertile, though redundancy of Ca_V3 isoforms could not be totally discarded as the double $Ca_V3.1/Ca_V3.2$ knockout mouse has not been evaluated.

Pharmacological and immunological evidence is consistent with the participation of Ca_V channels in the mouse sperm AR (reviewed in Darszon et al., 2011; Escoffier et al., 2010; Wennemuth et al., 2000). However, though T-type currents have been recorded in testicular mouse sperm (Martínez-López et al., 2008); neither L- or T-type channels have yet been electrophysiologically recorded in epididymal or more mature mouse sperm (Ren and Xia, 2010). Despite this, it has not been completely ruled out that the absence of Ca_V currents in epididymal sperm could be due to their down regulation during sperm maturation and reappearance after its capacitation.

Here we further explored the NA blockade mechanisms of T-type currents in native mouse spermatogenic cells and characterized its possible differential action on recombinant human Ca_V3 channels stably-expressed in HEK-293 cells. Our results show an IC_{50} for NA of around 74 μM in spermatogenic cells, but also indicate a different sensitivity of Ca_V3 isoforms to NA. $Ca_V3.2$ is the least NA sensitive isoform while $Ca_V3.1$ is the most sensitive isoform when expressed in HEK cells (Fig. 7). In addition, our molecular modeling of NA docking to the pore domain of Ca_V3 channels is in agreement with the strongest blockade being measured for $Ca_V3.1$ followed by $Ca_V3.3$ and $Ca_V3.2$ channels (Fig. 11*A*).

An estimate of the dissociation constant for the NA-channel complex using the current fractional block at 100 μM of NA for each channel yielded K_d values of 78.4, 192.0, and 137 μM for $Ca_V3.1$, $Ca_V3.2$ and $Ca_V3.3$, respectively. The corresponding value for the T-type current of spermatogenic cells was ~70 μM (59% block with 100 μM NA), very close to the IC_{50} obtained by fitting a Hill function to the experimental data of Fig. 1*A*. This evidence suggests that $Ca_V3.2$ might not be the only Ca_V channel present in spermatogenic cells, and could explain, at least in part, the remaining ~15% of the current insensitive to the higher concentration of NA used in this work (1 mM). Our results are in agreement with earlier reports indicating that $Ca_V3.2$ represents ~60% of the T-current (Trevino et al., 2004).

It is worth emphasizing that the mechanism of blockade of T-type channels by NA had not been explored in detail. The relationship between voltage-dependence of activation (Fig. 1*B* and 8*B*) and steady state-inactivation (Fig. 2) of recombinant and native T-type currents, suggests that NA blockade occurred at a site near to the vestibule of the channel that does not interfere with the channel voltage dependence. These evidences are consistent with the external binding site for NA proposed in several types of K^+ and HCN channels, although in such cases NA does alter the voltage dependence and the gating of the channels (Wang et al., 1997; Busch et al., 1994; Peretz et al., 2005; Accili and Difrancesco 1996; Satoh and Yamada 2001; Cheng and Sanguinetti 2009). We found that the blockade percentage of T-type currents by NA in spermatogenic cells was practically the same at all tested voltages, suggesting a blocking mechanism that does not interfere with the voltage sensitivity of the channel. This voltage independent blockade of T-type currents by NA is in agreement with the behavior observed in heterologously expressed $Ca_V3.2$ channels (Fig. 8*E*). $Ca_V3.1$ and $Ca_V3.3$ showed a discrete voltage dependence of blockade (Fig. 8*E*).

A striking difference between native and recombinant T-type channels was the effect of NA on their current kinetics. The time course of activation was slowed down in the T-type currents of spermatogenic cells and in all Ca_V3 channel isoforms. On the other hand,

inactivation was only affected in spermatogenic cells (Fig. 3 and 9). Also, the blockade magnitude was greater when native channels were kept inactivated, rather than when they were closed or deactivated. Thus, NA probably stabilizes the inactivated state of T-type channels, slowing their recovery from inactivation, since the drug takes longer to dissociate from the channel. In addition, as outward currents recorded at large depolarizations were poorly blocked by NA (Fig. 8), we suggest this compound binds to the outer vestibule of the channel. Since our dose response curve indicates a unique binding site, it probably also modulates the stability of the channel's inactivated state. Furthermore, the docking data also indicated that NA binds preferentially to the extracellular face of $Ca_V3.1$ channels and to the pore itself of $Ca_V3.3$ (Fig. 11). The latter result could explain the NA effects on the mild voltage-dependence of blockade percentage (Fig. 8*A*) and the slowing of the activation kinetics (Fig. 9*C*) of $Ca_V3.3$ channels. However, the delay in the recovery from inactivation observed in native (Fig. 5) and recombinant channels (Fig. 10), suggests an additional effect of NA in Ca_V3 channels. Such effect was more drastic in $Ca_V3.2$ channels, though the average docking energies were very similar in all the protein model clusters of this channel (Fig. 11*C*). In the absence of crystal structures of Ca_V3 channel proteins, the information obtained from channel modeling could be useful to obtain insights into the molecular binding of drugs to these channels, as has been already probed for other ion channels (Qadri *et al.*, 2010; Mancilla-Percino *et al.*, 2010; Lee *et al.*, 2011).

In summary, our findings contribute to a better understanding of how NA blocks Ca_V3 currents. The blockade by this non-steroidal anti-inflammatory drug is basically voltage independent and is more efficacious in the open and in the inactivated state than in the closed state of the T-type channels. $Ca_V3.1$ channels are the most sensitive Ca_V3 isoform to NA and their affinity is similar to that of the spermatogenic cell native T-type currents. The faster recovery from inactivation of the spermatogenic cell native T-type currents is also closer to that of $Ca_V3.1$ channels. Modeling of NA docking to Ca_V3 channels predicts that this compound preferentially binds to the extracellular face of $Ca_V3.1$ channels and to the pore itself of $Ca_V3.3$

Our present study shows that the biophysical properties of the T-type Ca^{2+} currents in mouse spermatogenic cells and their blockade by NA are closer to those displayed by heterologously expressed $Ca_V3.1$ channels. If so, how do we explain that spermatogenic cells from $Ca_V3.2$ null mice have no T-type currents (Escoffier et al., 2007), and those from $Ca_V3.1$ null mice have T-type currents with characteristics similar to those of native spermatogenic cells (Stamboulian et al., 2004)? The most parsimonious explanation is that the $Ca_V3.2$ isoform in these cells and testicular sperm may have some modified characteristics due to its sequence and/or regulation, in comparison with this same isoform from other mouse tissues (reviewed in Perez-Reyes et al., 2009; Darszon et al., 2011).

Under physiological conditions T-type channels would be mostly inactivated at the sperm resting membrane potential (~ −40 mV) and our findings indicate that this is the state with higher affinity for NA (IC_{50} ~70 μM). This characteristic is consistent with our previous observation that NA inhibits the progesterone induced mouse sperm AR with an IC_{50} of ~85 μM. However, NA inhibits the ZP induced AR at an IC_{50} of ~1 μM corroborating that the progesterone and ZP signaling pathways are different, and that other channels, possibly Ca^{2+}

regulated Cl^- channels are important for the ZP induced AR (Espinosa et al., 1998). Although recently it was shown that CatSper channels are potently activated by progesterone in human sperm, this does not occur in mouse sperm (Lishko et al., 2011; Strunker et al., 2011). Our results suggest that the higher progesterone concentrations (45 μM) needed to induce AR in these cells may activate other Ca^{2+} channels. Finally, it will be worth exploring if T-type channels participate in spermatogenesis.

Acknowledgments

We are grateful to Dr. Ignacio López-González for fruitful discussion, and to Dr. Chris Wood for reviewing this work.

Contract grant sponsor: Consejo Nacional de Ciencia y Tecnología (CONACyT).

Contract grant number: 49113 & 128566 (To A.D.) and J50250Q (to JC Gómora).

Contract grant sponsor: The National Institute of Health

Contract grant number: R01 HD 038082-07 A1 (To Pablo Visconti & Alberto Darszon)

Contract grant sponsor: Programa de Apoyo a Proyectos de Investigación e Innovación Tecnológica (PAPIIT).

Contact grant number: IN 211809210, IN 109210 & DGAPA IX 200910 (To A.D.)

References

Accili EA, DiFrancesco D. Inhibition of the hyperpolarization-activated current (if) of rabbit SA node myocytes by niflumic acid. Pflugers Arch. 1996; 431:757–762. [PubMed: 8596727]

Arnoult C, Cardullo RA, Lemos JR, Florman HM. Activation of mouse sperm T-type Ca2+ channels by adhesion to the egg zona pellucid. Proc Natl Acad Sci USA. 1996; 93:13004–13009. [PubMed: 8917534]

Benoff S, Chu CC, Marmar Jl, Sokol RZ, Goodwin LO, Hurley IR. Voltage-dependent calcium channels in mammalian spermatozoa revisited. Front Biosci. 2007; 12:1420–1449. [PubMed: 17127392]

Busch AE, Herzer T, Wagner CA, Schmidt F, Raber G, Waldegger S, Lang F. Positive regulation by chloride channel blockers of IsK channels expressed in Xenopus oocytes. Mol Pharmacol. 1994; 46:750–753. [PubMed: 7969055]

Cheng L, Sanguinetti MC. Niflumic acid alters gating of HCN2 pacemaker channels by interaction with the outer region of S4 voltage sensing domains. Mol Pharmacol. 2009; 75:1210–1221. [PubMed: 19218366]

Darszon A, López-Martínez P, Acevedo JJ, Hernández-Cruz A, Treviño CL. T-type Ca2+ channels in sperm function. Cell Calcium. 2006; 40:241–252. [PubMed: 16797697]

Darszon A, Nishigaki T, Beltran C, Treviño CL. Calcium channels in the development, maturation and function of spermatozoa. Physiological Reviews. 2011 (Accepted).

DeLano, WL. The PyMOL Molecular Graphic System. Palo Alto CA USA: DeLano Scientific; 2002.

Doyle DA, Morais CJ, Pfuetzner RA, Kuo A, Gulbis JM, Cohen SL, Chait BT, MacKinnon R. The structure of the potassium channel: molecular basis of K+ conduction and selectivity. Science. 1998; 280:69–77. [PubMed: 9525859]

Escoffier J, Boisseau S, Serres C, Chen CC, Kim D, Stamboulian S, Shin H-S, Campbell KP, De Waard M, Arnoult C. Expression, localization and functions in acrosome reaction and sperm motility of Ca(V)3.1 and Ca(V)3.2 channels in sperm cells: an evaluation from Ca(V)3.1 and Ca(V)3.2 deficient mice. J Cell Physiol. 2007; 212:753–763. [PubMed: 17450521]

Espinosa F, De la Vega-Beltran JL, Lopez-Gonzalez I, Delgado R, Labarca P, Darszon A. Mouse sperm patch-clamp recordings reveal single Cl2 channels sensitive to niflumic acid, a blocker of the sperm acrosome reaction. FEBS Lett. 1998; 426:47–51. [PubMed: 9598976]

Espinosa F, Lopez-Gonzalez I, Serrano CJ, Gasque G, De la Vega-Beltran JL, Trevino CL, Darszon A. Anion channel blockers differentially affect T-type Ca(2+) currents of mouse spermatogenic cells, alpha1E currents expressed in Xenopus oocytes and the sperm acrosome reaction. Dev Genet. 1999; 25:103–114. [PubMed: 10440844]

Fiser A, Sali A. Modeller: generation and refinement of homology-based protein structure models. Methods Enzymol. 2003; 374:461–491. [PubMed: 14696385]

Guha R, Howard MT, Hutchison GR, Murray-Rust P, Rzepa H, Steinbeck C, Wegner J, Willighagen EL. The Blue Obelisk-interoperability in chemical informatics. J Chem Inf Model. 2006; 46:991–998. [PubMed: 16711717]

Hamill OP, Marty A, Neher E, Sakmann B, Sigworth FJ. Improved patch-clamp techniques for high-resolution current recording from cells and cell-free membrane patches. Pflugers Arch. 1981; 391:85–100. [PubMed: 6270629]

Jagannathan S, Punt EL, Gu Y, Arnoult C, Sakkas D, Barratt CL, Publicover SJ. Identification and localization of T-type voltage-operated calcium channel subunits in human male germ cells. Expression of multiple isoforms. J BiolChem. 2002; 277:8449–8456.

Ji H, Delker SL, Li H, Martasek P, Roman LJ, Poulos TL, Silverman RB. Exploration of the active site of neuronal nitric oxide synthase by the design and synthesis of pyrrolidinomethyl 2-aminopyridine derivatives. J Med Chem. 2010; 53:7804–7824. [PubMed: 20958055]

Krissinel E. Crystal contacts as nature's docking solutions. J Comput Chem. 2010; 31:133–143. [PubMed: 19421996]

Lee JH, Lee Y, Ryu H, Kang DW, Lee J, Lazar J, Pearce LV, Pavlyukovets VA, Blumberg PM, Choi S. Structural insights into transient receptor potential vanilloid type 1 (TRPV1) from homology modeling, flexible docking, and mutational studies. J Comput Aided Mol Des. 2011; 4:317–327. [PubMed: 21448716]

Lievano A, Santi CM, Serrano CJ, Trevino CL, Bellve AR, Hernandez-Cruz A, Darszon A. T-type Ca2+ channels and alpha1E expression in spermatogenic cells, and their possible relevance to the sperm acrosome reaction. FEBS Lett. 1996; 388:150–154. [PubMed: 8690075]

Lishko PV, Botchkina IL, Kirichok Y. Progesterone activates the principal Ca2+ channel of human sperm. Nature. 2011; 471:387–381. [PubMed: 21412339]

Mancilla-Percino T, Correa-Basurto J, Trujillo-Ferrara J, Ramos-Morales FR, Acosta Hernandez ME, Cruz-Sanchez JS, Saavedra-Velez M. Molecular modeling study of isoindolines as L-type Ca(2+) channel blockers by docking calculations. J Mol Model. 2010; 16:1377–1382. [PubMed: 20151167]

Martínez-López P, Santi MC, Treviño CL, Ocampo-Gutierrez AY, Acevedo JJ, Alisio A, Salkoff LB, Darszon A. Mouse sperm K+ current stimulated by pH and cAMP possibly coded by Slo3 channels. Biochem Biophysical Res Com. 2008; 381:204–209.

Morris GM, Godsell DS, Halliday RS, Huey R, Hart WE, Belew RK, Olson AJ. Automated docking using a Lamarckian genetic algorithm and empirical binding free energy function. J Comput Chem. 1998; 19:1639–1662.

Park JY, Ahn HJ, Gu JG, Lee KH, Kim JS, Kang HW, Lee JH. Molecular identification of Ca2+ channels in human sperm. ExpMol Med. 2003; 35:285–292.

Peretz A, Degani N, Nachman R, Uziyel Y, Gibor G, Shabat D, Attali B. Meclofenamic acid and diclofenac, novel templates of KCNQ2/Q3 potassium channel openers, depress cortical neuron activity, and exhibit anticonvulsant properties. Mol Pharmacol. 2005; 67:1053–1066. [PubMed: 15598972]

Perez-Reyes E. Molecular physiology of low-voltage-activated T-type calcium channels. Physiol Rev. 2003; 83:117–161. [PubMed: 12506128]

Perez-Reyes E, Van Deusen AL, Vitko L. Molecular pharmacology of human Cav3.2 T-type Ca2+ Channel: Block by Antihypertensives, Antiarrhytmics and their analogs. JPET. 2009; 328:621–627.

Qadri YJ, Song Y, Fuller CM, Benos DJ. Amiloride docking to acid-sensing ion channel-1. J Biol Chem. 2010; 285:9627–9635. [PubMed: 20048170]

Ren D, Xia J. Calcium signaling through CatSper channels in mammalian fertilization. Physiology Bethesda. 2010; 25:165–175. [PubMed: 20551230]

Roy A, Kucukural A, Zhang Y. I-TASSER: a unified platform for automated protein structure and function prediction. Nat Protoc. 2010; 5:725–738. [PubMed: 20360767]

Sanner MF. Python: a programming language for software integration and development. J Mol Graph Model. 1999; 17:57–61. [PubMed: 10660911]

Santi CM, Darszon A, Hernandez-Cruz A. Dihydropyridine sensitive T-type Ca2+ current is the main Ca2+ current carrier in mouse primary spermatocytes. Am J Physiol. 1996; 271:1583–1593.

Satoh TO, Yamada M. Niflumic acid reduces the hyperpolarization activated current (Ih) in rod photoreceptor cells. Neurosci Res. 2001; 40:375–381. [PubMed: 11463484]

Sherman SM. Thalamic relays and cortical functioning. Prog Brain Res. 2005; 149:107–126. [PubMed: 16226580]

Son WY, Han CT, Lee JH, Jung KY, Lee HM, Choo YK. Developmental expression patterns of alpha1H T-type Ca2+ channels during spermatogenesis and organogenesis in mice. Dev Growth Differ. 2002; 44:181–190. [PubMed: 12060068]

Son WY, Lee JH, Lee JH, Han CT. Acrosome reaction of human spermatozoa is mainly mediated by alpha1H T-type calcium channels. Mol Hum Reprod. 2000; 6:893–897. [PubMed: 11006317]

Stamboulian S, Kim D, Shin HS, Ronjat M, De Waard M, Arnoult C. Biophysical and pharmacological characterization of spermatogenic T-type calcium current in mice lacking the CaV3.1 (alpha1G) calcium channel: CaV3.2 (alpha1H) is the main functional calcium channel in wild-type spermatogenic cells. J Cell Physiol. 2004; 200:116–124. [PubMed: 15137064]

Steriade M. Sleep, epilepsy and thalamic reticular inhibitory neurons. Trends Neurosci. 2005; 28:317–324. [PubMed: 15927688]

Strunker T, Goodwin N, Brenker C, Kashikar ND, Weyand I, Seifert R, Kaupp UB. The CatSper channel mediates progesterone-induced Ca2+ influx in human sperm. Nature. 2011; 471:382–386. [PubMed: 21412338]

Trevino CL, Felix R, Castellano LE, Gutierrez C, Rodriguez D, Pacheco J, Lopez-Gonzalez I, Gomora JC, Tsutsumi V, Hernandez-Cruz A, Fiordelisio T, Scaling AL, Darszon A. Expression and differential cell distribution of low-threshold Ca(2+) channels in mammalian male germ cells and sperm. FEBS Lett. 2004; 563:87–92. [PubMed: 15063728]

Trott O, Olson AJ. Auto Dock Vina: improving the speed and accuracy of docking with a new scoring function, efficient optimization, and multi threading. J Comput Chem. 2010; 31:455–461. [PubMed: 19499576]

Wang HS, Dixon JE, McKinnon D. Unexpected and differential effects of Cl− channel blockers on the Kv4.3 and Kv4.2 K^+ channels. Implications for the study of the I_{to2} current. Circ Res. 1997; 81:711–718. [PubMed: 9351445]

Wennemuth G, Westenbroek RE, Xu T, Hille B, Babcock DF. CaV2.2 and CaV2.3 (N- and R-type) Ca2+ channels in depolarization-evoked entry of Ca2+ into mouse sperm. J BiolChem. 2000; 275:21210–21217.

Zhou Y, Morais-Cabral JH, Kaufman A, MacKinnon R. Chemistry of ion coordination and hydration revealed by a K+ channel-Fab complex at 2.0 A resolution. Nature. 2001; 414:43–48. [PubMed: 11689936]

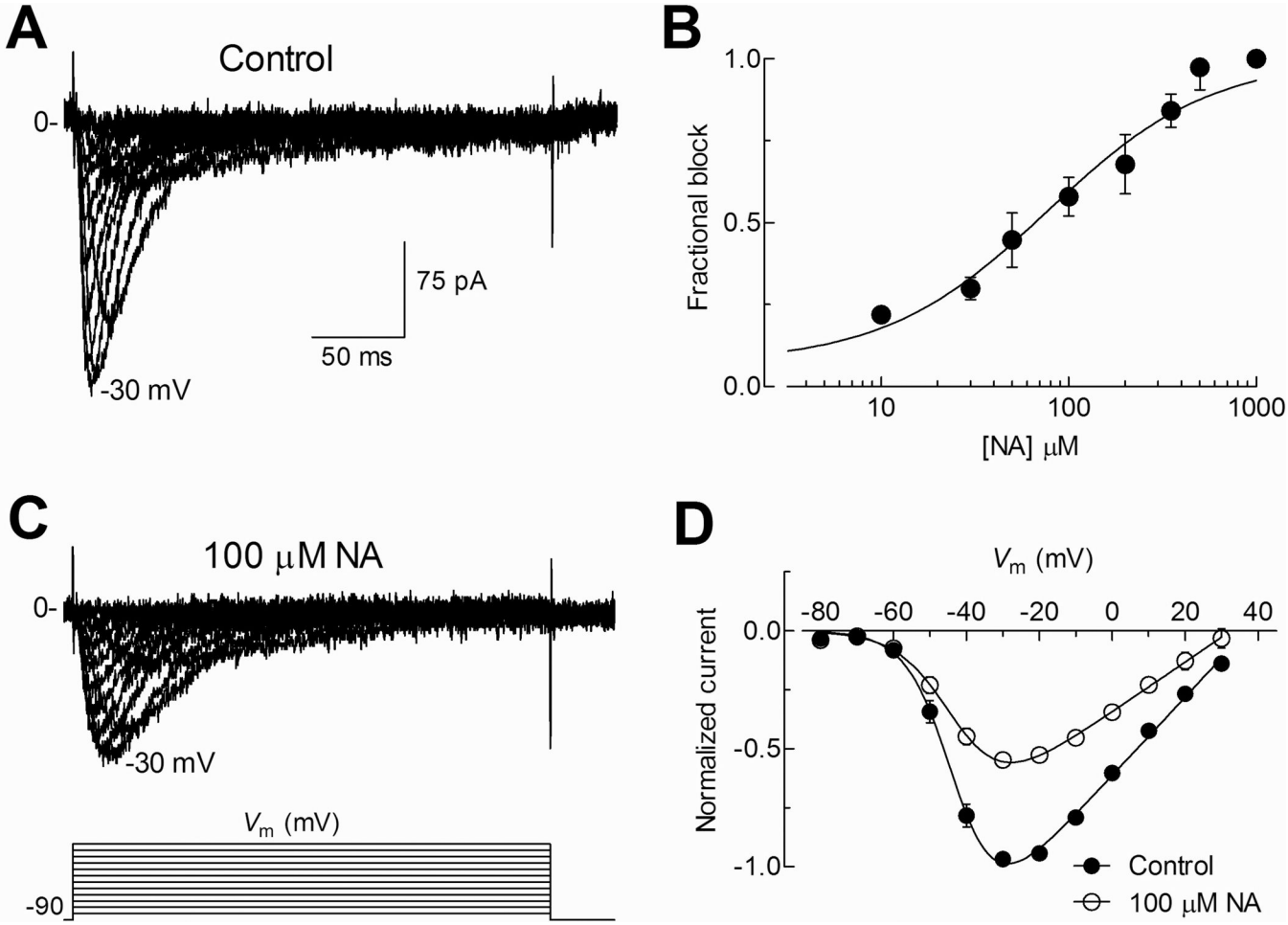

Fig. 1. Blockade of T-type currents by NA in mouse spermatogenic cells

A) A family of currents recorded in whole cell configuration in control conditions in response to depolarized pulses from a −80 to +70 mV in +10 mV increment from a HP of −90 mV (traces from −80 to +30 mV are show for clarity). *B*) Dose-response curve. Data points are (mean ± SEM) the fraction of blocked current at −20 mV for each NA concentration tested. Fit of experimental points with a Hill equation (solid line) produces an estimated IC_{50} for NA of 73.5 μM. *C*) Currents recorded as in (*A*) but in the presence of 100 μM NA. *D*) Current-voltage (*I–V*) curve was constructed with the peak current normalized and averaged from 12 individual cells under control (filled circles) and in presence of 100 μM NA (open circles). In both conditions, threshold of currents was observed around −60 mV.

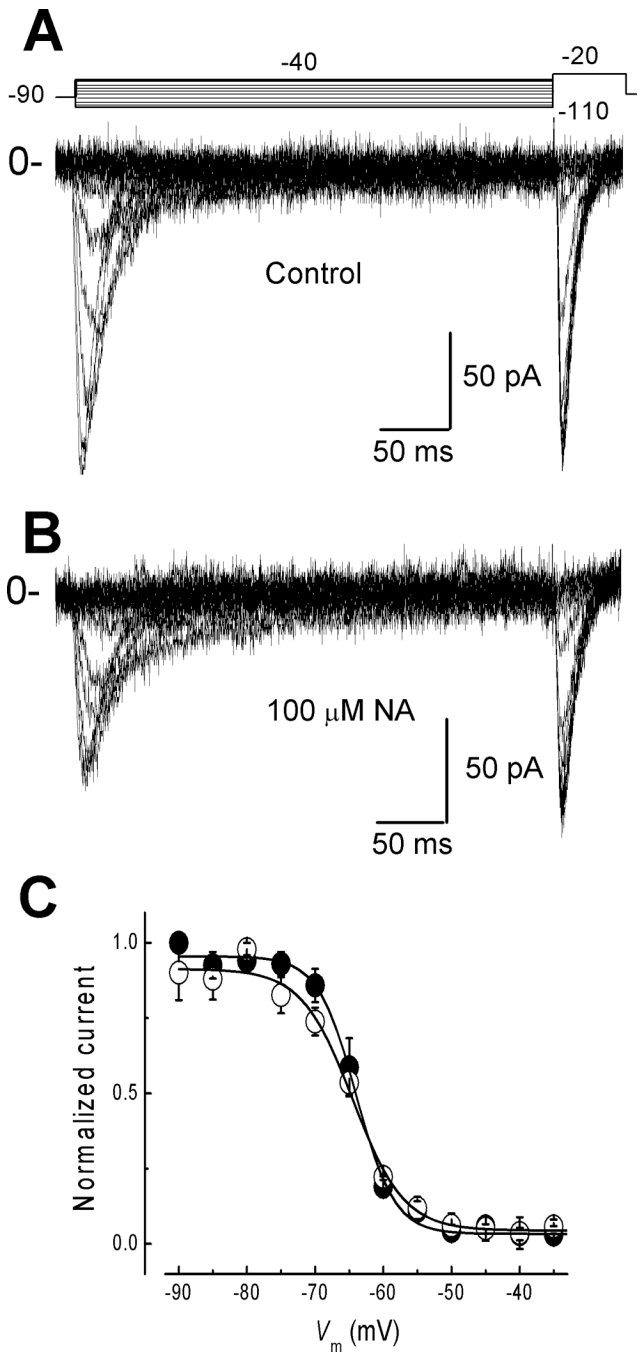

Fig. 2. Steady-state inactivation of spermatogenic cell T-type currents is not affected by NA

A) Family of currents recorded with the voltage protocol depicted at the top. Channels were inactivated with 350-ms prepulses to potentials between −110 and −40 mV in 5 mV steps, from a HP = −90 mV. Then, channel availability was tested at −20 mV. *B*) Family of currents recorded as in A, but in presence of 100 μM NA. *C*) Steady-state inactivation curves in the absence and the presence of NA. Data points show the normalized peak amplitude of currents elicited under control (filled circles) and NA (open circles) by the testing pulse at −20 mV, and plotted against the prepulse potentials. Continuous lines are the

best fits with a Boltzmann function. Values of V_{50} and k obtained from this curves are summarized in Table 1.

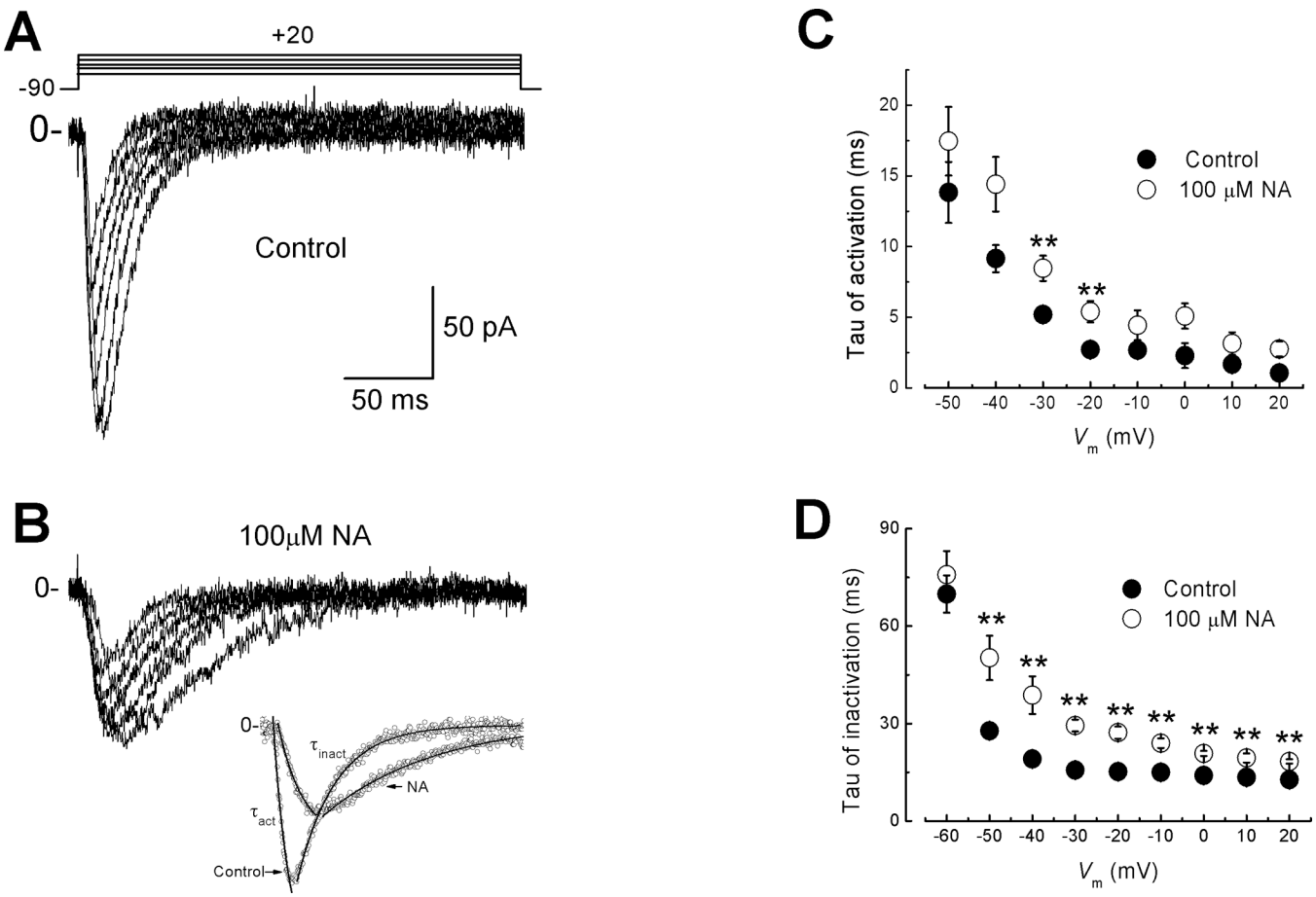

Fig. 3. Effect of NA on the activation and inactivation kinetics of T-type currents

A) Calcium currents recorded under control conditions with the voltage protocol displayed at the top. *B*) Same as in A, but in presence of 100 μM NA. Tau of activation (τ_{act}) and tau of inactivation (τ_{act}) were obtained by fitting single exponentials to the traces as shown at the inset. *C*) Plot of mean values for τ_{act} against command voltage (n = 6). Control condition is represented by filled symbols and NA by open circles. *D*) Plot of mean values for τ_{inact} in control (filled circles) and NA (open circles) against test potential (n = 6). Note that NA induced a slow down effect on the current inactivation kinetics at all potentials more positive than −50 mV. Bars represent SEM.

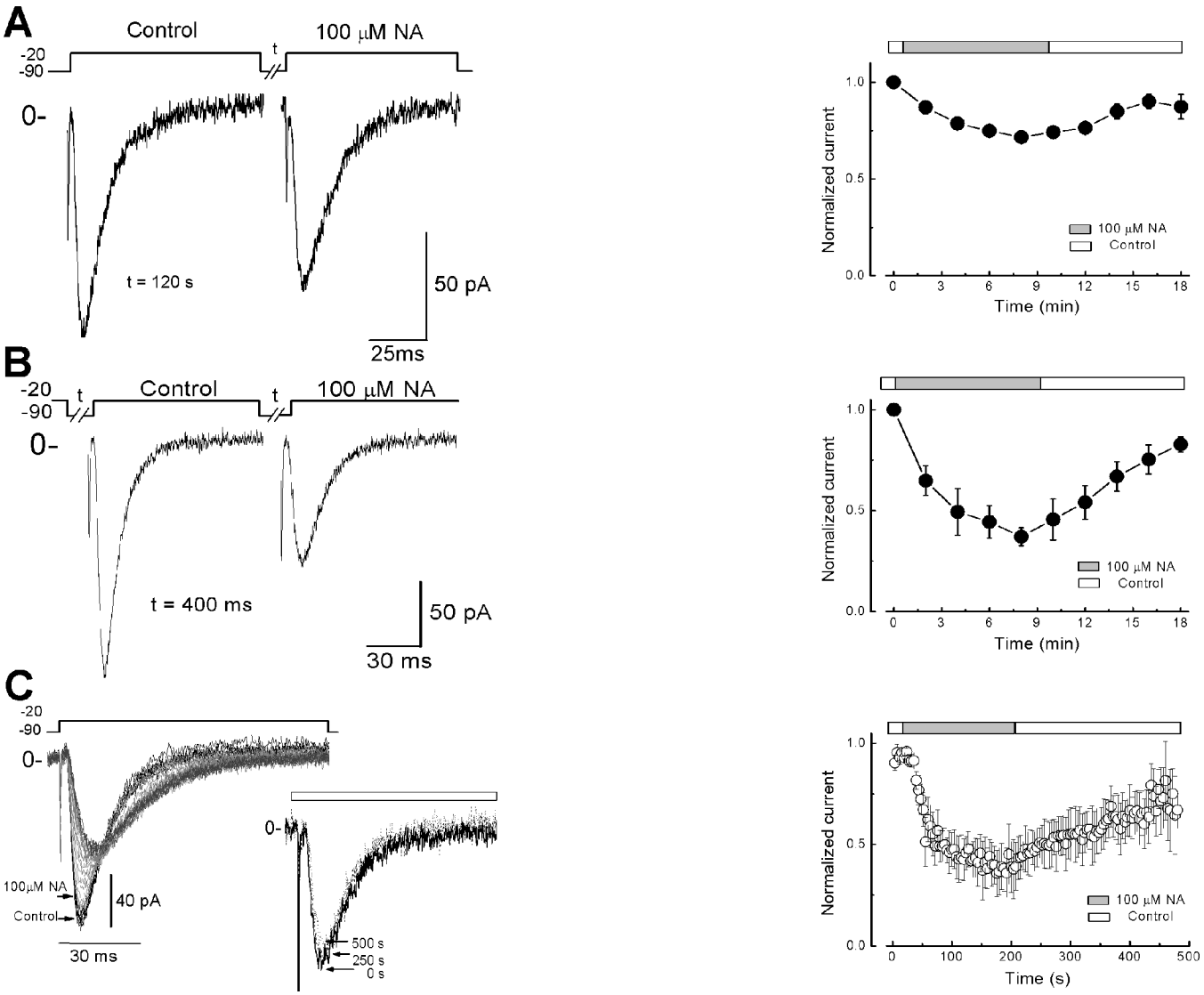

Fig. 4. NA Blockade of T-type channels is state-dependent

A) *Left panel*, traces of current recorded with the protocol depicted above to maintain the T-type channels in the closed state. A test pulse of −20 mV was applied with at = 120 s from a HP = −90 mV. *Right panel*, normalized current was plotted against time; white and grey bars represent time to exposure to control solution and NA, respectively. Note that ~ 25% of inward current amplitude was reduced by NA. *B*) Effect of NA on inactivated state of T-type channels. *Left panel*, current recorded in response to a depolarization to −20 mV from a 400 ms hyperpolarized pulse to −90 mV. Cells were held at −20 mV to maintain the channels inactivated. *Right panel* normalized current versus time of exposure to NA. Note a reduction of more than 50% in presence of the drug by using the inactivated state protocol. *C*) *Left panel*, blockade of T-type currents by NA in open state. Cells were clamped at −90 mV during the whole experiment with a depolarization to −20 mV with a Δt = 5 s. *Inset*, continuously stimulated cells with the protocol previously described during 500 s without drug did not modify the currents during the whole experiment. *Right panel*, normalized current shows a decrement in the amplitude of the current of more than 50% during the time

of exposure. Error bars represent SEM, (n = 6). Note that in the three conditions 85% of the original current was recovered by washing the drug.

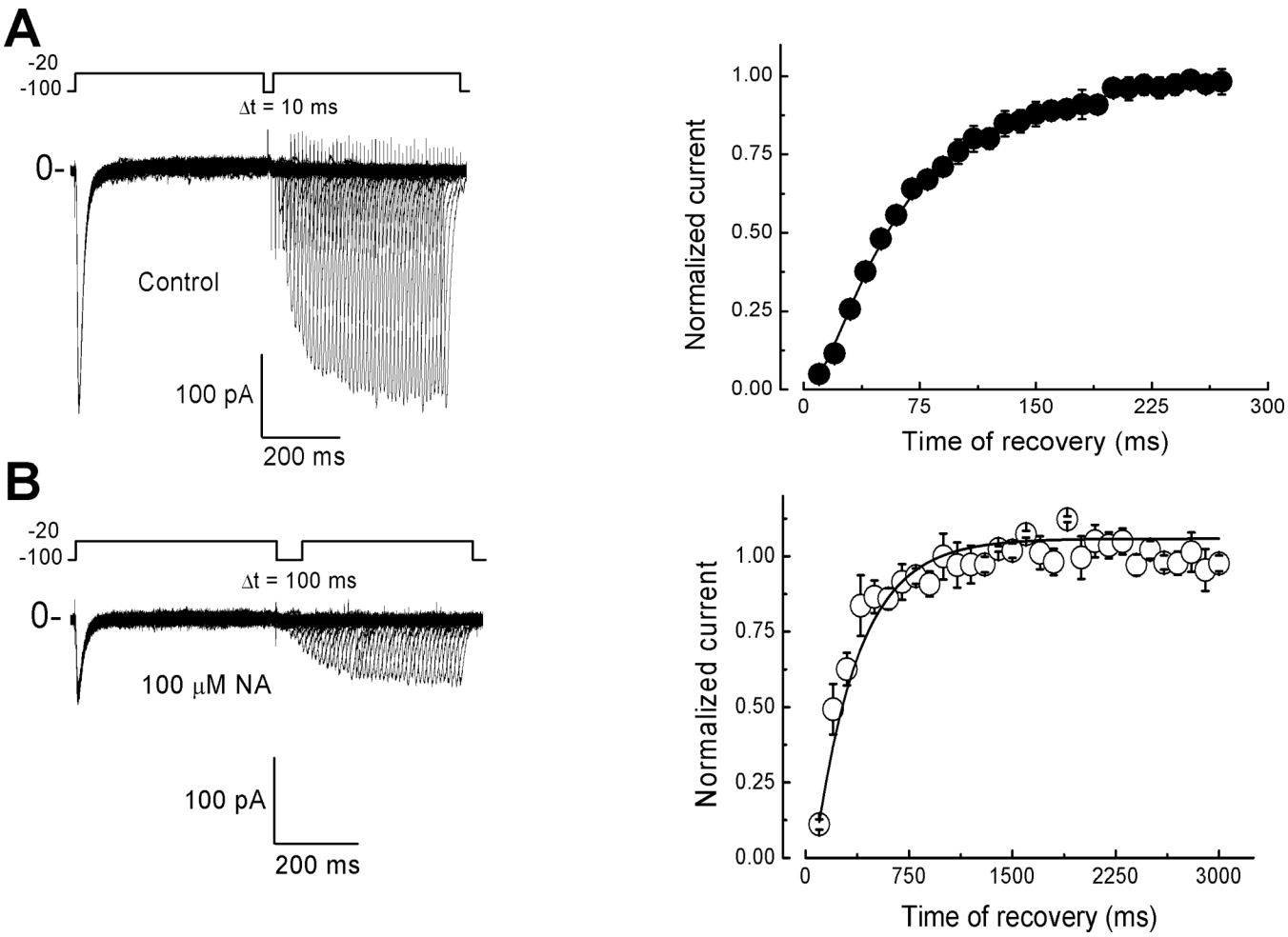

Fig. 5. NA delays recovery from inactivation of T-type channels

Current traces recorded with two pulses voltage protocol, depolarizing pulses to −20 mV from a HP = −100 mV were applied at different inter-stimulus interval (Δt), 10 ms increments for control condition (*A*), and 100 ms for NA (*B*). Time courses of recovery from inactivation (*right panels*) were fitted by single exponential functions with time constant (τ_h) of 67.6 ± 3.05 ms for control (*A*) and 318.01 ± 20.5 ms in the presence of 100 μM of NA (*B*). Error bars represent SEM (*n* = 9).

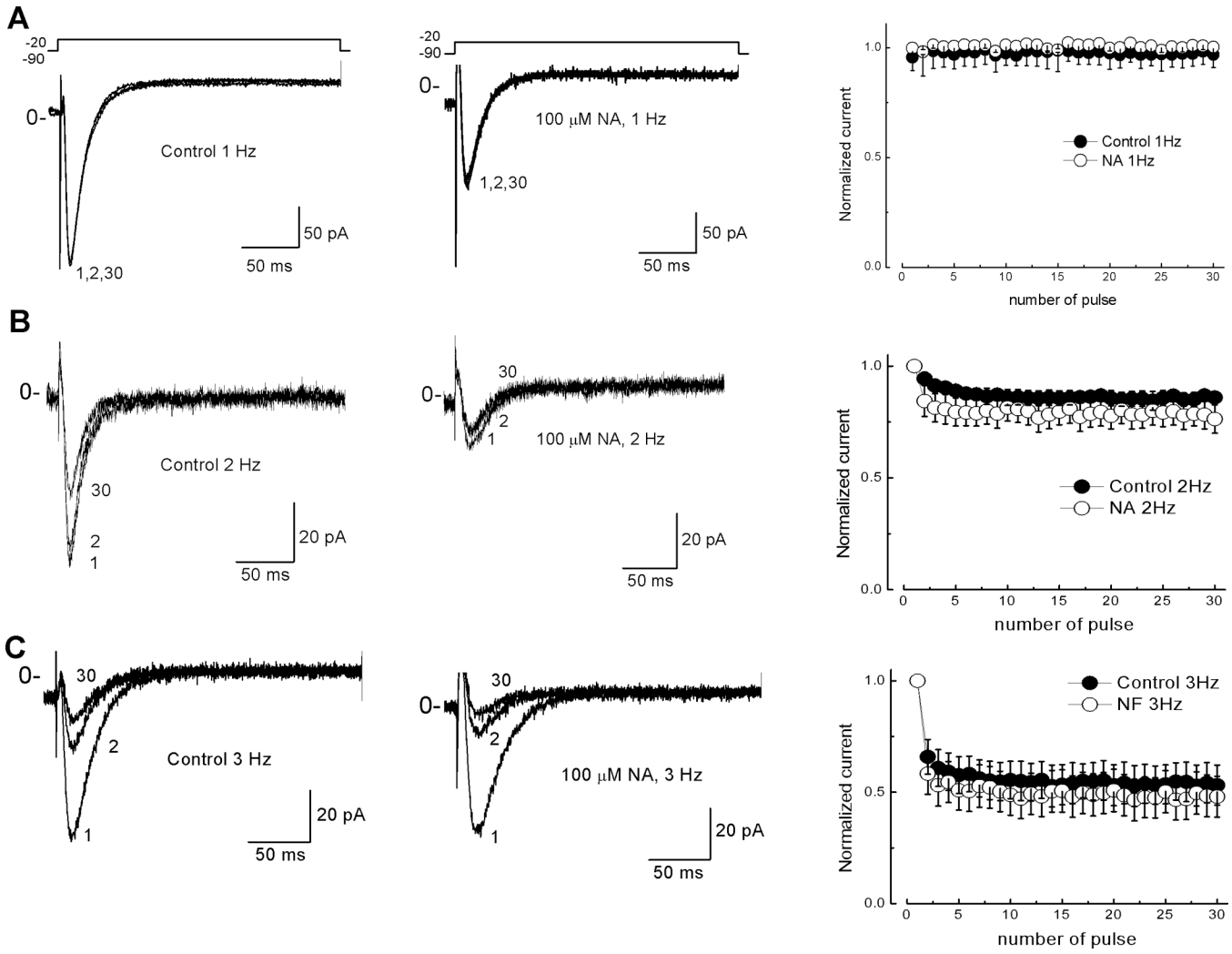

Fig. 6. Blockade of T-type channels by NA is not use dependent

Cells were stepped to −20 mV from a HP of −90 mV with a stimulation frequency of 3 (*A*), 2 (*B*), and 1 (*C*) Hz. Under control (*left panels*) and 100 μM NA condition (*middle panels*). Only pulses 1, 2 and 30 are shown for illustrative purposes. *Right panels*, plots of normalized current against time for control (filled circles) and NA (open circles) in the three frequencies tested. Note that reduction of ~35 % in the current was due to the accumulation of inactivation at least in 3 and 2 Hz. Error bars represent SEM (n = 6).

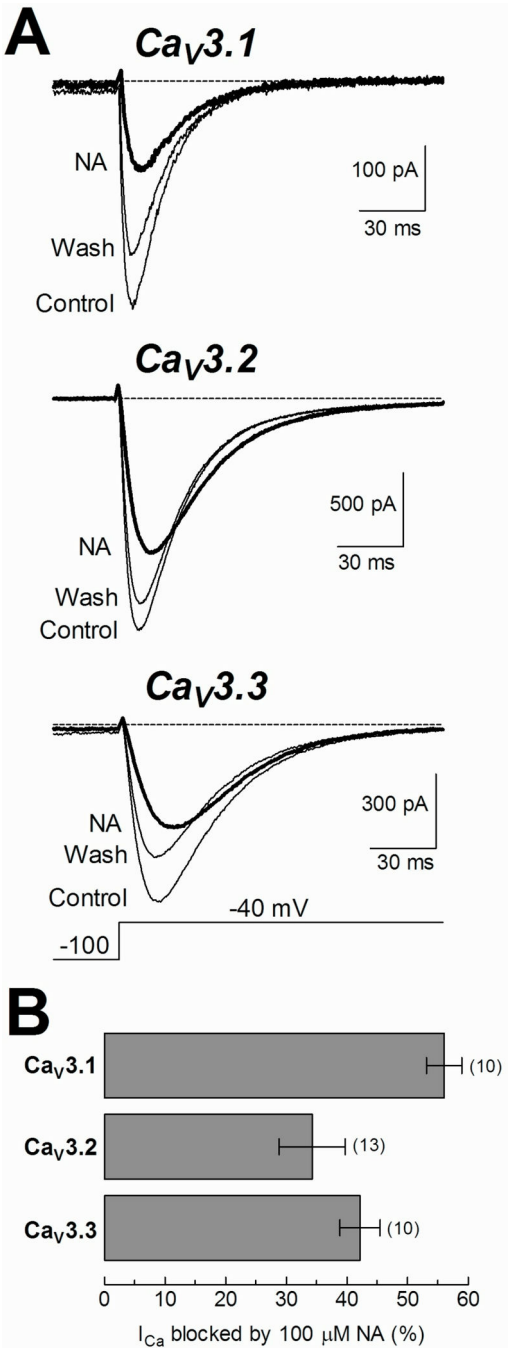

Fig. 7. Recombinant Ca_V3 channels are sensitive to NA

A) Examples of calcium currents recorded at −40 mV before (Control), during (NA, thick trace), and after (Wash) exposure to 100 μM NA from HEK-293 cells stably expressing $Ca_V3.1$, $Ca_V3.2$ and $Ca_V3.3$ channels. Depolarization steps lasted 300 ms, although for clarity, only the first 150 ms are shown. *B*) Blockade percentage of peak calcium currents at −40 mV induced by 100 μM NA in Ca_V3 channels. The NA blockade percentage was calculated for each cell, averaged and plotted as a mean ± SEM for each type of channel.

The respective values were 56 ± 3, 34 ± 5 and 42 ± 3% for $Ca_V3.1$, $Ca_V3.2$ and $Ca_V3.3$, respectively. The number of assayed cells is indicated in parentheses.

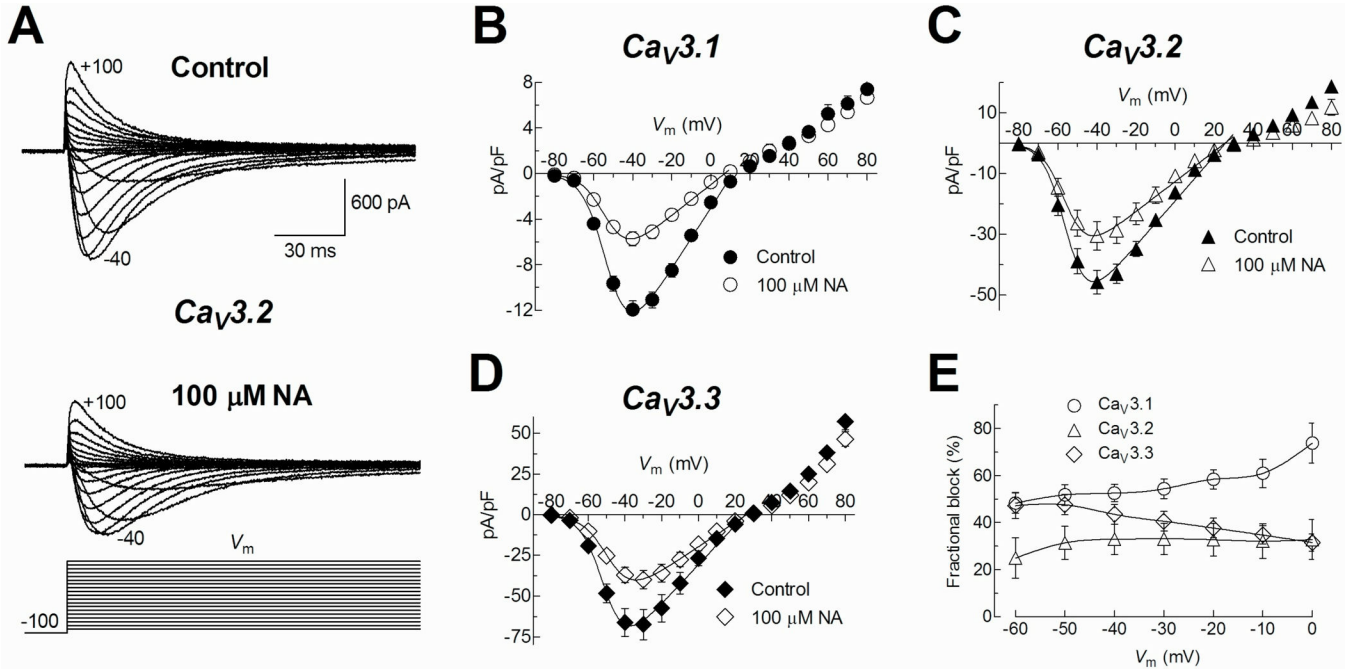

Fig. 8. NA blockade of recombinant Ca_V3 channels is voltage-independent

A) Representative family of traces obtained in Control and 100 μM NA experimental conditions. Currents were recorded from a HEK-293 cell expressing $Ca_V3.2$ channels in response to the *I–V* protocol illustrated at the bottom. *B–D*) Current-voltage relationships for $Ca_V3.1$, $Ca_V3.2$, and $Ca_V3.3$ channels, respectively, in the absence (Control) and the presence of 100 μM NA. Data points representing inward currents were fitted with a modified Boltzmann function (continues line) and the obtained parameters are summarized in Table 1. Note that the amplitude of outward currents was practically unaffected by the presence of NA. *E*) Blockade percentage of Ca_V3 channels by NA and V_m relationships. The blockade percentage of peak current by NA was calculated for each potential. Data was obtained from 7 ($Ca_V3.1$), 6 ($Ca_V3.2$) and 5 ($Ca_V3.3$) HEK-293 cells.

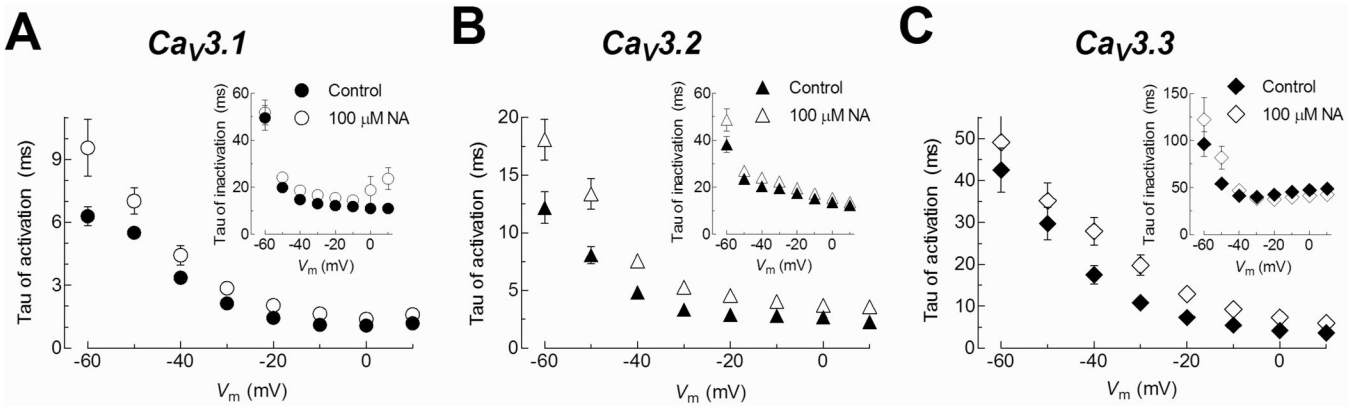

Fig. 9. Current activation kinetics of Ca$_V$3 channels is slowed down by NA

Current recordings as shown in Fig. 8*A* were fitted by the sum of two exponentials, one for activation and the other for current decay. The resulting time constants (taus) were plotted as function of the test potential for each channel as indicated. The larger modifications were observed in the current activation of Ca$_V$3.2 and Ca$_V$3.3 channels. *Insets*: Tau of inactivation *versus* test potential for the same channels.

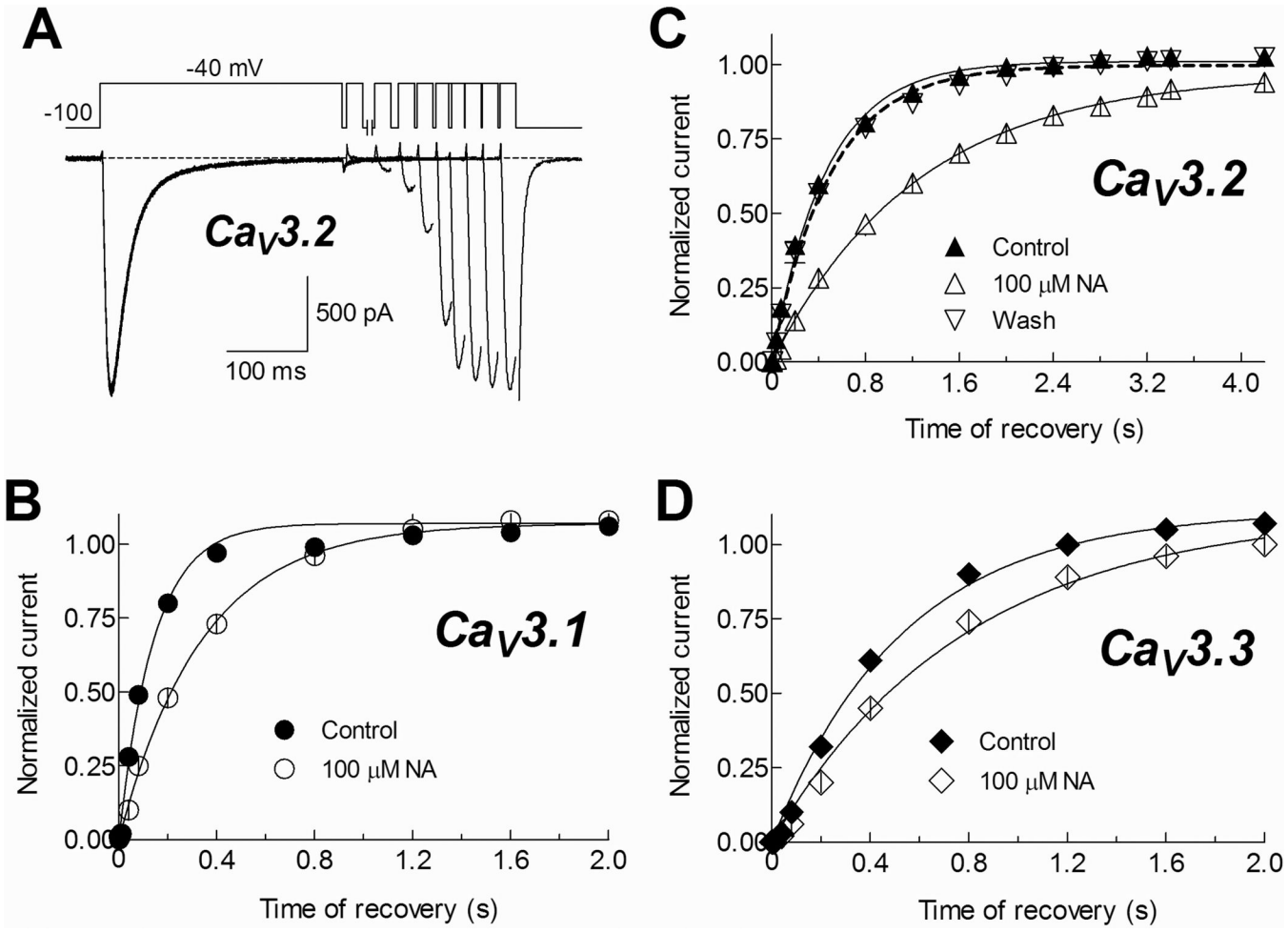

Fig. 10. Recovery from inactivation of recombinant Ca$_V$3 channels is drastically modified by NA

A) Recovery from inactivation at −100 mV of Ca$_V$3.2 channels in control conditions. The two-pulse protocol used is shown at the top. Ca^{2+} currents were inactivated by a 300 ms pulse to −40 mV, after which the membrane potential was stepped to −100 mV for periods ranging from 1 to 4200 ms, at that time a 20 ms activating voltage step to −40 mV was applied. Only current traces at −40 mV obtained after 5, 40, 80, 200, 800, 1600, 2400, 3200 and 4200 ms at −100 mV are shown, and only the tail current (generated by repolarizing at −100 mV) of the latter is partially plotted. *B–D*) Time course of recovery from inactivation at −100 mV for the indicated Ca$_V$3 channels in Control and 100 μM NA conditions. The values are the peak current during the 20 ms pulse, normalized to the peak current in the 300 ms pulse. Data were pooled from 6 (Ca$_V$3.1), 6 (Ca$_V$3.2) and 5 (Ca$_V$3.3) HEK-293 cells. Smooth curves are fits to the data using a one phase exponential association equation. Dashed line in (*C*) corresponds to the same kind of fit to data from 3 cells where current recovery from NA blockade was above 90%. Tau values are given in Table 1.

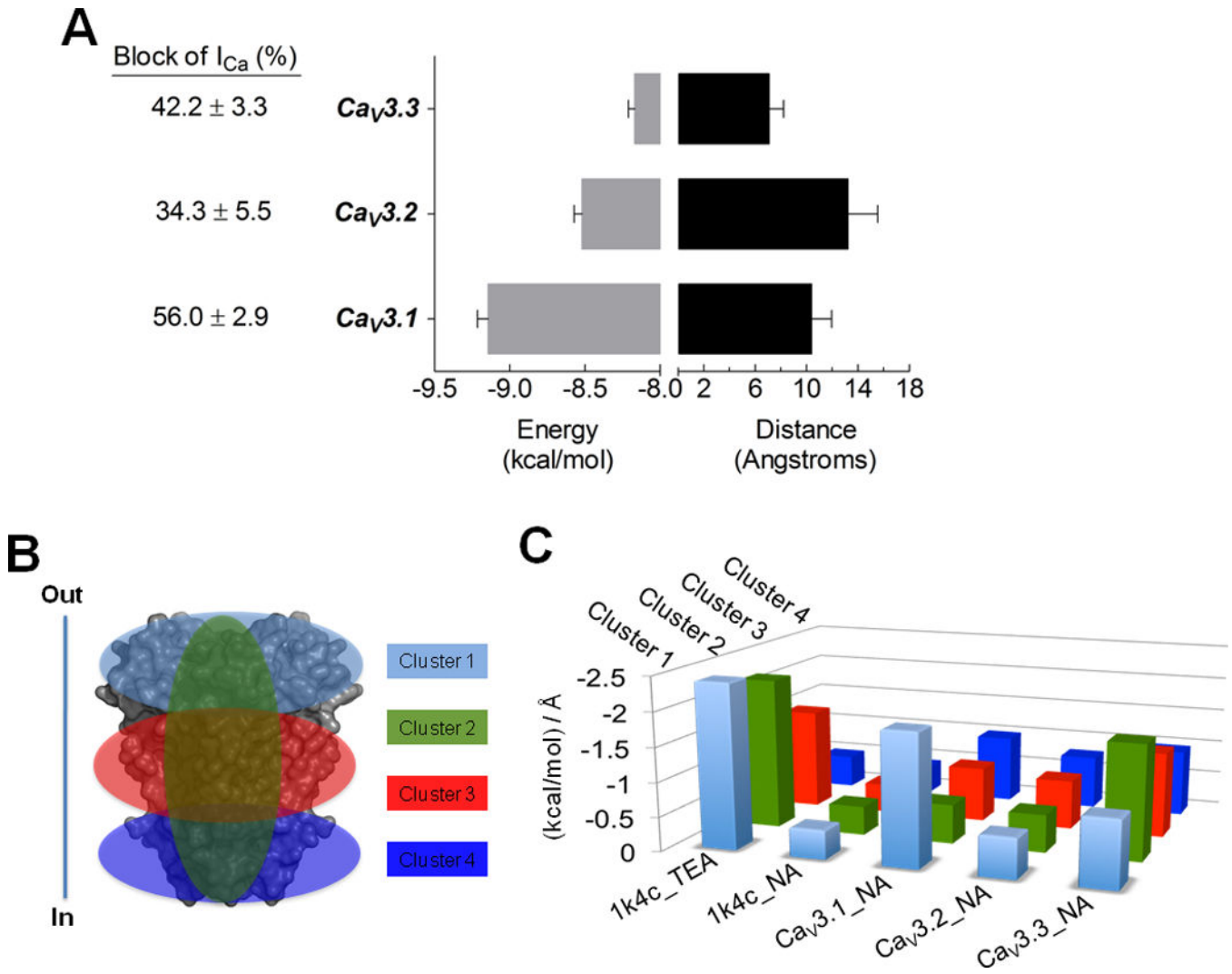

Fig. 11. Niflumic acid docking to Ca_V3 channels

A) Average binding energies (kcal/mol) and distance (in Å, Angstroms), for niflumic acid (NA) as ligand docked to Ca_V3 pore domain models. Distance data was obtained from RMSD l.b. values, which is the relative value to the best mode using only movable heavy atoms or lower bound. Columns are averages of the minimum or best binding energy for the docking results. The 1K4C coordinates were used as control for the interaction with TEA. NA docked with 1K4C showed a low interaction value (~ −0.4), serving as low affinity control. Error bars represent SEM from n = 36 interaction models of each Ca_V3 channel. *B*) Docking analysis was clustered as shown, in order to search the whole grid spacing of the protein models and control structures. *In* and *Out* denote the intra and extracellular side of the cell. *C*) The ratio between kcal/mol and RMSD l.b. (in Å) for each cluster are illustrates as follows: cluster 1, clear blue, involves the upper region of the proteins; cluster 2, green, the pore; cluster 3, red, the middle transmembrane region of the proteins; and cluster 4, dark blue, the intracellular region of the protein.

Table 1

Voltage and kinetic parameters of native and recombinant Ca_V3 channels in the absence and the presence of 100 μM NA.

	Spermatogenic cells T-type current		$Ca_V3.1$		$Ca_V3.2$		$Ca_V3.3$	
	Control	**NA**	**Control**	**NA**	**Control**	**NA**	**Control**	**NA**
V_{50}	−42.7 ± 0.6	−42.3 ± 1.2	−52.3 ± 0.9	−52.8 ± 1.5	−55.2 ± 1.0	−55.6 ± 1.7	−50.7 ± 1.5	−48.1 ± 1.8
k	6.2 ± 0.4	7.4 ± 0.8	6.0 ± 0.6	6.0 ± 1.0	5.6 ± 0.7	5.8 ± 1.3	6.1 ± 1.1	6.9 ± 1.2
V_{rev}	36.9 ± 1.4	32.5 ± 2.0	11.2 ± 1.4	7.0 ± 2.1	25.7 ± 1.9	25.3 ± 3.3	25.4 ± 2.6	26.2 ± 2.7
τ_{act}	2.7 ± 0.4	4.4 ± 1.0	3.4 ± 0.2	4.4 ± 0.5	4.9 ± 0.3	7.6 ± 0.6 *	17.5 ± 2.2	27.9 ± 3.3 *
τ_{inact}	15.2 ± 1.0	27.2 ± 1.9 *	14.8 ± 0.7	18.6 ± 1.4	20.4 ± 1.2	24.1 ± 1.9	41.4 ± 1.9	47.0 ± 4.9
τ_h	68 ± 3	318 ± 21 *	143 ± 4	340 ± 10 *	525 ± 12	1246 ± 50 *	533 ± 19	785 ± 52 *

Data are mean ± SEM. V_{50}, k, and V_{rev} are given in mV and were obtained from *I–V* relationship fits with the modified Boltzmann functions. τ_{act} and τ_{inact} are shown in ms, and were obtained from two exponential fits of current recordings at −20 mV (native channels) or at −40 mV (recombinant channels). τ_h was obtained from single exponential fits to the recovery from inactivation data at −100 mV, and is also presented in ms. The number of investigated cells were 9 for spermatogenic cell channels; 7 for $Ca_V3.1$, 7 for $Ca_V3.2$, and 6 for $Ca_V3.3$ channels for all parameters, except for τ_h where the number of cells were 6 ($Ca_V3.1$), 6 ($Ca_V3.2$) and 5 ($Ca_V3.3$).

Asterisks denotes statistical significance when using a Student´s *t* test (P <0.05).